6-2003

Fluorescence in ultraviolet active binaries: the case of FF Aquarii

Todd R. Vaccaro
St. Cloud State University, trvacarro@stcloudstate.edu

R. E. Wilson
University of Florida

Mon. Not. R. Astron. Soc. **342,** 564–574 (2003)

Fluorescence in ultraviolet active binaries: the case of FF Aquarii

T. R. Vaccaro[1,2]★ and R. E. Wilson[2]

[1]*Department of Physics and Astronomy, Louisiana State University, Baton Rouge, LA 70803-4001, USA*
[2]*Astronomy Department, University of Florida, Gainesville, Florida, 32611, USA*

Accepted 2003 February 21. Received 2003 February 16; in original form 2002 October 25

ABSTRACT

The eclipsing binary FF Aquarii (FF Aqr) consists of a small hot star of uncertain type and a red giant. An Hα feature varies from absorption during eclipse to maximum emission during hot star transit. We have obtained simultaneous differential photometry in *BVRI* bands and Hα spectroscopy in 1998 that covered an entire orbit with some overlap. A binary star model was used with our light-curve, radial velocity and Hα data to refine stellar and orbital parameters. A new ephemeris indicates that the period has increased or is longer than previously thought. A physically simple algorithm is developed that generates properly blended spectral line profiles of binaries with arbitrary combinations of surface emission and absorption line regions. Although there is no radiative transfer, the algorithm can accommodate modest geometrical intricacy. For now, all line broadening in the model is rotational. The algorithm has now been incorporated within the general Wilson-Devinney binary star model, and we used it to model FF Aqr's photospheric iron profile. It also is used to generate templates that illustrate problems with FF Aqr's strongly time-dependent Hα emission profiles, which appear to be blends of features from the photosphere and from above the photosphere. The dominant broadening mechanism should be rotation for individual line components. Absorption profiles were generated by the model and fit to the observations to yield a red star radius $\approx$6.9 $R_\odot$, which then requires $i \approx 76^\circ$. Our light-curve models have five spots with temperatures $\approx$1000 K cooler than the surrounding photosphere. Hα emission was modelled on the red star surface, centred at the substellar point to simulate a fluorescent chromosphere. Additional emission is seen outside our modelled profiles. The origins of this excess emission may be corotating prominences, winds, or coronal mass ejections, all of which could affect the orbit period.

Key words: stars: activity – binaries: close – circumstellar matter – stars: magnetic fields – stars: spots – stars: winds, outflows.

1 INTRODUCTION

Ultraviolet (UV) active binaries offer opportunities to study strongly irradiated atmospheres, so the unusual system FF Aquarii (FF Aqr) was a primary target in our photometric and spectroscopic program to investigate the role of fluorescence in UV active binaries. The UV source in this case is a hot component, perhaps contracting on its way to a later stage or possibly a helium star, that we call the primary. The secondary component is cool (G8 to K0) and shows enhanced solar-like activity. Dark spots, bright plages, and some flares are detectable photometrically. The secondary's activity is expected in view of its tidally induced rapid rotation. The binary is detached, with a UV point source as a probe of a red giant outer atmosphere in a system free of rapid mass transfer effects.

The size disparity between components accounts for the overwhelming luminosity of the secondary at visible and infrared wavelengths, and it is easy to observe at long wavelengths without contamination from the hot primary. Eclipsing systems of this type provide two distinct aspects of the secondary: that of the undisturbed larger star during primary eclipse, and that of an illuminated region around the inferior conjunction of the small primary. The chromosphere of the cool star absorbs incident UV radiation, leading to ionization of hydrogen with subsequent recombination and emission (i.e. fluorescence). The Hα line is one of the strongest produced in this process, well isolated from the light of the hot star in the visual range, and easily observed from the ground. The line should vary regularly in strength and profile as the illuminated hemisphere rotates in and out of view.

Fluorescence modelling is a logical step toward understanding chromospheric radiative processes that produce cyclic spectral signatures (orbital cycle). However, additional emissions are intrinsic to the secondary, such as lines of Ca II (H + K), Mg II (h + k) and Hα that are clear indicators of an active chromosphere (Bopp & Talcott 1980). Mechanisms for these emissions could be linked to magnetic

★E-mail: vaccaro@rouge.phys.lsu.edu

structures above photospheric spots and plages (Young, Skumanich & Paylor 1988). These regions are known to be activity centres for events such as flares and prominences that may vary synchronously with a star-spot cycle in strength and frequency.

The binary nature of FF Aqr was first suspected upon its detection as a UV source with a K0 spectrum (Carnochan et al. 1975). A photometric and spectroscopic investigation by Dworetsky et al. (1977) identified the star as an eclipsing and chromospherically active binary. Their *U* photometric analysis covered the 1975 and 1976 observing seasons and yielded a 9.2-d orbital period, *P*. A deep primary eclipse, a notable 'reflection' bump at phase ≈ 0.5, and variations outside the eclipse are main features of their light curve. The red star was found to be G8III on its heated, inner-facing hemisphere, and K0III on the outer-facing hemisphere, while the hot star was said to be consistent with an O or B subdwarf (but see Section 5). Dorren, Guinan & Siah (1983) report from unpublished *v,b,y* light curves that much of the variation is due to dark spots. Their light-curve models had the K star covered nearly 42 per cent with spots 800 K cooler than the surrounding photosphere in 1977 and 1978. A later analysis along with *International Ultraviolet Explorer* (*IUE*) observations gave the masses and radii as 2.0 $M_\odot$ and 5.7 $R_\odot$ for the giant star and 0.5 $M_\odot$ and 0.14 $R_\odot$ for the hot star while assuming $i = 81^\circ$ (Etzel et al. 1988). Etzel (1989) noted a sudden *P* increase, based on 1986, 1987 and 1988 photometry. A longer *P* or *P* increase was noted by Marilli et al. (1995) as the reason for the lack of eclipse coverage in new light curves. Marilli et al. also present clear evidence of phase-dependent Hα emission that peaks when the hot star is in front of the giant. It is this emission we have modelled as fluorescence. We have also looked into the problematic and possibly changed or changing *P*, which could provide insight into activity and evolution. Exploratory early aspects of this work have been shown in two meeting posters (Vaccaro & Wilson 1999a,b).

2 THE NEW DATA

Photometric and spectroscopic observations were made at Kitt Peak National Observatory (KPNO) from 1998 October 29 to November 9. Spectra were obtained with the Coudé Feed 0.9-m telescope. CCD images were taken with the 0.9-m telescope of the Southeastern Association for Research in Astronomy (SARA), which is also located at the KPNO facility. This arrangement allowed simultaneous photometric and spectroscopic coverage. Most nights were fairly clear with only a few partially ruined by clouds, high winds, humidity, or fog.

2.1 Photometry

The SARA telescope was equipped with a CCD camera with a 9-arcmin^2 field of view and filters that reproduce the standard Johnson *B*, *V*, *R* and *I* bands reasonably well. Pixels were double binned into 1024 × 1024 images. This resolution (0.53 arcsec per pixel) sufficiently sampled the slightly out-of-focus stellar images and avoided overexposure, while the binning also reduced the data size for storage. The comparison star (BD -3°5358) fit within the field so that program and comparison stars were imaged in a single exposure. Three exposures were taken with each filter before cycling to the next one. Exposure times varied with the filter and ranged from a typical 7 s in *I* to 40 s in *B*. The frames were processed with the Image Reduction and Analysis Facility software (IRAF), which is made available by the National Optical Astronomy Observatories. The standard IRAF task DAOPHOT for aperture photometry was used. The seeing was rarely as good as one arc second and many of the images were somewhat out of focus so a large aperture with a radius of 15 pixels was used for all of the frames. There were no problems with stellar crowding so a five pixel wide annulus (2.6 arcsec) around this aperture was used to sample the background sky. Differential magnitudes between FF Aqr and the comparison star were produced for each frame with typical nightly mean errors of $\approx$0.005 mag.

Twilight sky flats were taken, but the most useful flats came from sky images during a time of dense fog. These 'fog' flats became the standard flats by which most of the data were reduced. Technical difficulties degraded or even invalidated some of the photometric data. Anomalous data were thrown out if the observing log indicated any technical or atmospheric problems. The instrumental magnitudes of the comparison stars were plotted against airmass to evaluate and reject abnormal data due to clouds or obstruction by the dome.

Table 1. Radial velocity lines.

Element	Wavelength (Å)
Fe	6400.000
Fe	6408.030
Fe	6411.647
Fe	6546.239
Fe	6625.021
Fe	6663.440
Ca	6439.075
Ca	6449.808
Ca	6462.567
Ni	6643.630

2.2 Spectroscopy

The Coudé Feed telescope was equipped with the F3KB CCD camera, grating A, and the long collimator. Exposures of 30–45 min had typical signal-to-noise ratio (S/N) of $\approx$70, dispersion of 0.12 Å pixel^{-1}, and covered $\approx$300 Å centred near 6525 Å. A Th–Ar comparison lamp was imaged at the beginning, end, and sometimes the middle of each night for wavelength calibration. The spectra were reduced with standard IRAF techniques, normalized to the continuum level, and Doppler shifted so as to be heliocentric. Telluric lines were not removed and one appears near the middle of Hα, posing as a disk feature; however, the position and strength of the line is consistent with a telluric feature at 6564 Å. Another telluric line at 6572 Å can be used as a reference as to the strength of the interloping line at 6564 Å. We suspect these lines to be water vapour that also appear in the spectra of HR533, which is a B star with few stellar absorption lines.

Radial velocities were measured with the IRAF RV package. Table 1 shows the photospheric lines used in determining radial velocities for the red giant. The flux bisection method (the IRAF CENTER1D task) for finding the line centres was used, as the Gaussian profile fitting algorithm does not work well with distorted profiles. Each spectrum's velocity was determined from approximately 10 lines.

3 ANALYSIS OF NEW AND EARLIER DATA

3.1 Data sets from multiple epochs – overall prospects

Analysis was hampered by several factors. FF Aqr is clearly rife with activity that can be seen in both our photometry and spectra. Our observations only cover 1.2 orbits, so cycle-to-cycle variations could not be encountered. *P* seems longer than originally published

by Dworetsky et al. (1977) as we expected to cover the eclipse but did not. Descent into or rise from totality, if caught, would have given good timing information and allowed refinement of the ephemeris. Eclipse depth would have given a tighter constraint on relative temperature. A significant deficiency was lack of colour coverage around phase ≈0.5, where a reflection bump is seen and where we obtained only *B* data. Because of competition with variation due to star-spots, the reflection amplitude cannot be estimated well without measures in other bands. Star-spot parameters (temperature, size and position) thereby become more uncertain. There is also the issue of the amplitude of ellipsoidal variation due to tidal distortion of the giant, which primarily depends on the size of the giant compared to its limiting lobe, $R_2/R_{\rm lobe}$. Alternatively we can say that it depends on the combination of mass ratio, q, and relative size, R_2/a, where a is the semimajor axis length for the relative orbit. We are dealing with a single-lined binary as there are no published hot star velocities, although q values of 4.0 (Etzel et al. 1988) and ≈4.5 (Marilli et al. 1996) are indicated by unpublished velocities from *IUE* data and yield masses consistent with the spectral and luminosity types.

Some of the data have shortcomings. According to Frasca (private communication), the velocities of Marilli et al. (1995), observed in 1990 and 1991, are not photospheric. They also do not match the points in the velocity solution figure of Marilli et al. (1995) and are offset from velocities sent by Frasca for many coincident HJDs by an average of about +20 km s^{-1}, suggesting that they may not be heliocentric (although the observation *times* are listed as heliocentric). The 25 photospheric velocities from Frasca include additional data from 1990 to 1994, are distributed over 4.2 yr, and have errors ≈10 km s^{-1}. The photometry of Dworetsky et al. (1977) was only shown graphically and the data have not been made available. We extracted the data point by point from a scan of their plot and scaled them in pixel space. The measurements were converted from phase to time with the ephemeris in that publication, and all data thus synthesized were placed in one cycle near the middle of the time window of the actual observations. (Dworetsky et al. analysed their radial velocities but did not tabulate or illustrate them.) The light curve spanned two observing seasons and their fig. 2 has many overlapping points, which made extraction difficult.

Our initial concern was with the ephemeris, so that we could correctly follow the phase dependence of the Hα line profile. Furthermore, changes in P could be linked to matter outflows and magnetic braking. The influence of spots on the light curves and the lack of eclipse coverage prevents use of our photometry to refine the ephemeris, but our radial velocities are useful for timing. The differential corrections routine (DC, Wilson & Devinney 1971; Wilson 1979, 1990) is written to process light and velocity data together so as to achieve coherent solutions and optimize the use of mixed data for ephemerides. These preliminary light/velocity solutions were made without use of line profile information. Simultaneous DC solutions included our velocities, those from Frasca, and the 1975–76 *U* photometry. The initial epoch (T_0 = HJD 244 2752.9577) and period (P = 9.207 755 d) of the old ephemeris were the starting points for iterations, and a, P, T_0 and systemic velocity (V_γ) were free parameters. The known radial velocity curves appear sinusoidal and our trial solutions found no evidence for eccentricity, so we assumed $e = 0$. A small eccentricity would not change our overall results significantly. The giant star potential was free so as to fit the eclipse width. The radii are not uniquely determined without use of line profile information as they depend on i and on a, while the nearly rectangular eclipse leaves i poorly determined, and only single lined velocities are used. Initially included was the free parameter $\mathrm{d}P/\mathrm{d}t$, which turned out to be nil within its standard error of $\approx 1 \times 10^{-7}$, so we assumed that $\mathrm{d}P/\mathrm{d}t = 0$. However, P is longer than that of Dworetsky et al. (1977) thereby explaining why we missed the eclipse. A check against the light curve of Marilli et al. (1995) is similarly consistent. Parameter results will be given in Section 3.4 for final solutions that made use of line profiles, which help break the indeterminacy among R_2, i and a.

3.2 A model for multiple blended emission and absorption lines

Three kinds of potentially useful red giant line profile modelling are:

(i) a reference absorption profile for the shielded (non-irradiated) region;

(ii) a combined emission/absorption profile that varies as spot-related Hα emitting regions pass in and out of view;

(iii) the combined emission/absorption profile of the irradiated region that also varies with aspect.

Only (i) and (iii) are applied here, but (ii) should be useful for cases with better time coverage. Although it may be useful to think of (i), (ii) and (iii) separately, they can be unified in applications. All can be evaluated with a scheme developed for FF Aqr and conceptually similar binaries that has now been made part of the public Wilson–Devinney (WD) program[1] (Wilson & Devinney 1971; Wilson 1979, 1990). The profiles are for rotation only, although other broadening mechanisms will be added later. This present limitation is not much of a drawback for FF Aqr, where rotation is by far the main broadening mechanism. The scheme is physically simple in that it does not incorporate stellar atmosphere modelling via radiative transfer theory, although it can represent rather intricate distributions of absorption and emission regions to first order, as blending of mixed emission and absorption regions is incorporated. Blending of multiple spectral lines also is incorporated, although we did not need that capability for FF Aqr. Lines can originate from an entire star or from designated circular subareas. Thus, a star can have arbitrary combinations of absorption line and emission line subareas, and the subareas can overlap. The areas may be eclipsed in the general case, although that effect is not significant for FF Aqr. Spectra are formed by bin sharing, which means that adjacent bins and even strips of bins can share contributions from a given surface element so as to eliminate quantizing error at bin edges. Bin sharing is implemented by having a rectangle of finite width as the plotting element. Contributions from a given surface element do not go exclusively to one bin but are shared among adjacent bins. In the simplest case, the width of the plotting element is the same as the bin width, so that just two adjacent bins share 100 per cent of the light from a surface element. Bin sharing helps greatly in producing smooth profiles. Another feature for smoothing profiles is subtiling of surface elements, whereby a subtiling integer n is specified and each element is subdivided into n^2 subelements, each with its own local radial velocity. The binned elements (not to be confused with the bins) are rectangles of specified width and depth (or height for emission lines). Absorption lines are specified by their equivalent widths and depths and are combined in terms of optical depth, τ, in a reversing layer. Emission lines are directly specified by emission line flux relative to a unit continuum, $f_{\rm e} = F_{\rm e}/F_{\rm c}$ (input). The

[1] The WD program can be downloaded from the anonymous FTP site ftp.astro.ufl.edu, subdirectory pub/wilson/lcdcprog.

narrow rectangles we now use for intrinsic profiles will later be refined to include several kinds of intrinsic broadening (primarily damping and thermal Doppler broadening). Relations for computing radial velocities of surface elements are given, for example in Wilson & Sofia (1976) and references therein. Rotation-only profiles are adequate for FF Aqr, as the red star is a fast-rotating, low-temperature giant and the line we model is due to iron. Low temperature and high atomic weight both lead to narrow thermal profiles, with mean iron atom speeds of about 1.5 km s^{-1}, while fast equatorial rotation of 38 km s^{-1} assures a wide overall profile dominated by rotation. Damping is also unimportant as we do not model any strong lines and there are no hints of damping wings in the observed profiles. The equivalent width of the iron line is estimated to be about 0.235 Å from fits to the spectra.

For a spectral bin with contribution d F_c to continuum flux from an arbitrary surface element, the dimensionless net flux excess or deficiency relative to the continuum is

$$\Delta f = \frac{\int_{\text{surface}} (1 - e^{-\tau} + f_e)\, \mathrm{d}F_c}{\int_{\text{surface}} \mathrm{d}F_c}, \quad (1)$$

where 'surface' refers to the instantaneously visible surface and fluxes are defined at the observer's location (by integration over the 'visible' face of each star, including tides, rotation, limb darkening, gravity brightening, reflection, and other effects treated by physical eclipsing binary programs such as WD). Here τ is a sum over all relevant absorption lines ($\tau = \Sigma\tau_i$) and f_e is a sum over all relevant emission lines ($f_e = \Sigma f_{e_i}$). Quantity $1 + \Delta f$ is then rescaled for best fit to a spectrum. Because the procedure is one of profile modelling rather than a full stellar atmosphere with radiative transfer, equivalent widths are those that best reproduce observed lines. Further details are in the documentation for WD (see footnote on WD access).

3.3 Observed versus computed red star photospheric profiles

Profile modelling of rotationally broadened photospheric lines allowed us to estimate the absolute size of the giant and further restrict parameters. Small adjustments in i have little effect on the rotational $V \sin i$, which is largely determined by the physical radius, under the assumption of constant angular velocity. A model absorption feature was checked against an observed Fe I line at 6400.0 Å. With rotation locked to that of the orbit, the giant's radius controls profile width. We altered the giant's potential (effectively its size) while keeping all other parameters fixed. A good subjective fit was obtained with $R_2 = 6.9\ R_\odot$ while adopting a preliminary i of 81° (Fig. 1) from Etzel et al. (1988). Thus the width of the 6400.0-Å line gives a handle on the absolute size of the giant. The i and a need re-adjustment to fit the eclipse for any assumed q. A fit to our velocities of Table 2 is shown in Fig. 2.

Table 2. Heliocentric radial velocities of FF Aqr.

HJD −245 1100	$V_r \pm$ mean error (km s^{-1})	HJD −245 1100	$V_r \pm$ mean error (km s^{-1})
15.62803	51.0±2.5	22.60174	19.1±1.2
15.65073	48.8±1.7	22.62338	16.5±1.5
15.70520	47.5±1.9	22.64442	18.3±1.0
16.60070	48.7±1.0	22.66548	19.2±0.9
16.63943	47.4±2.6	23.61841	32.3±1.2
16.66342	45.4±1.9	23.63956	32.7±1.6
17.68470	39.6±1.9	23.66070	33.6±1.5
18.59748	22.8±1.2	24.58680	49.5±2.1
18.62578	19.4±2.3	24.60809	49.3±2.0
19.61335	4.3±1.1	24.62915	44.5±1.8
19.63439	4.0±2.2	25.59452	47.5±2.2
19.65542	5.8±1.5	25.61557	47.5±1.6
20.61777	10.1±1.5	25.65004	49.1±1.6
20.63880	9.1±1.6	26.60746	41.4±2.2
20.65984	9.1±1.5	26.63321	38.1±2.3
21.63420	−2.4±1.9	26.65766	44.8±1.7

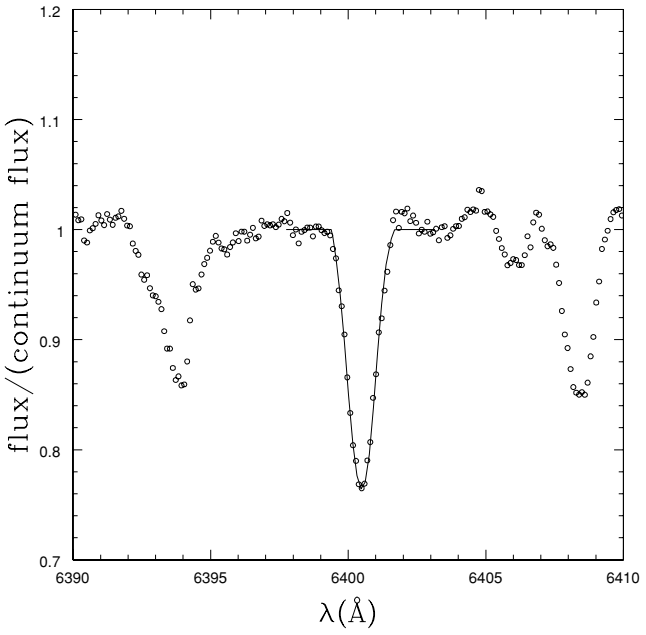

Figure 1. Observed spectrum of FF Aqr at $\phi = 0.52$ p (open circles) and the modelled Fe line at 6400 Å (solid line).

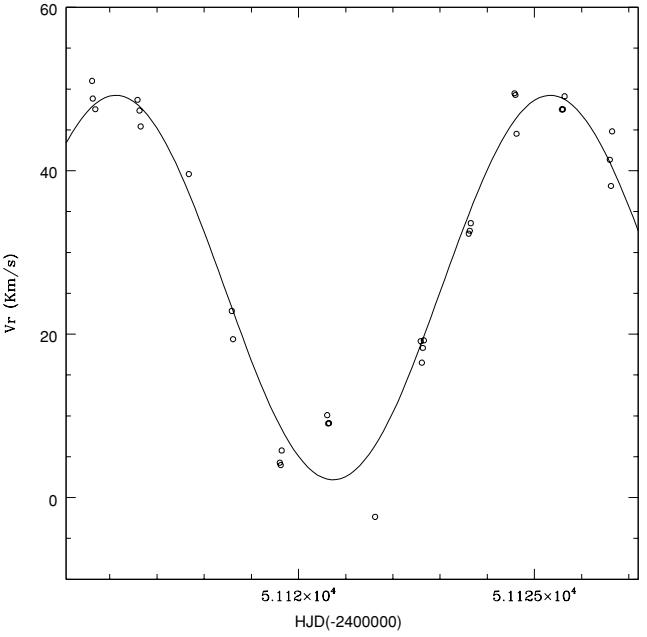

Figure 2. The model radial velocity curve (solid line) and our observed velocities (open circles).

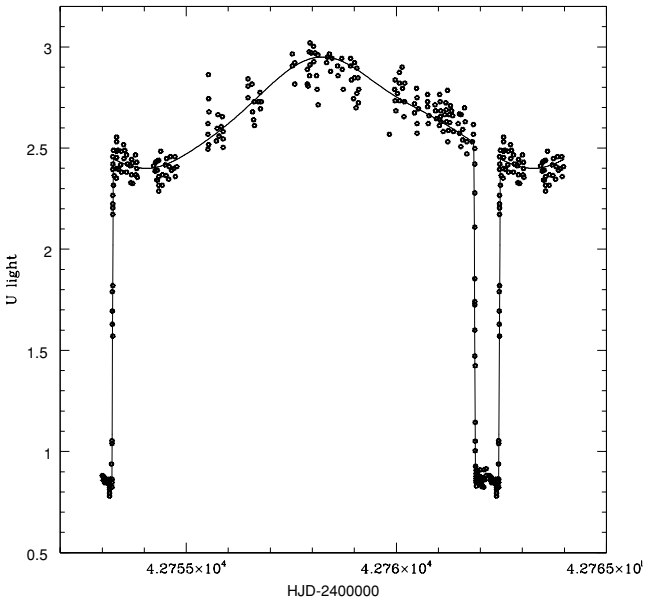

Figure 3. Our fit to the 1975–76 *U* light curve of Dworetsky et al. (1977).

3.4 Light/*RV* solutions consistent with line profiles

Light-curve models have been compared to the *U* photometry of Dworetsky et al. (1977) – see Fig. 3 – to check eclipse geometry. A large spot near the pole was needed, with the solution being primarily for fitting the eclipse. As there is no way to find q accurately from existing data, we stepped through a sequence of q ($q = 3.5$, 4.0 and 4.5), with the requirement that i fit the light curves for a giant radius $\approx$6.9 $R_\odot$. The temperatures were assumed to be $T_1 =$ 42 000 K and $T_2 = 4758$ K. The giant's temperature was estimated from typical G8III and K0III temperatures (Allen 2000). The hot star temperature is necessarily high to fit the eclipse and is within the range considered in the previous literature. In no sense can it be said that we have determined or even estimated T_1, considering that it correlates strongly with R_1/a (formally with Ω_1), and R_1/a is only weakly determined by the scanned light curves of Dworetsky et al. (1977). The situation would be improved if there were access to the unpublished photometry, as the partial eclipse phases that essentially measure R_1/a are much better defined in the original data. All solutions are based on a blackbody approximation and logarithmic limb darkening with coefficients by Van Hamme (1993). The simultaneous light/velocity solutions for the $q = 3.5$, 4.0, 4.5 sequence are in Table 3, where relative radii, $r = R/a$, are given as one number for the virtually spherical primary and for four places on the slightly distorted giant. The fact that the standard errors on inclination are very small is a formal consequence of Ω_2 being fixed to agree with photospheric line width. The realistic uncertainty in i is much larger because i and Ω_2 are highly correlated. A physical radius for each star, $R_1/R_\odot$ and $R_2/R_\odot$, is the radius of a sphere of equal volume. Masses for each q also are listed.

3.5 Dark star-spots at the 1998 epoch

Our light curves cannot be used to estimate the main geometric parameters because they do not include an eclipse, but they can tell about star-spots if we assume the geometry from Table 3. We fit our photometric data with model light curves using the parameters of Table 3 for $q = 4.0$. No satisfactory fit was possible without star-spots, so cool spots were added one at a time, with typical temperature factors, $T_{\rm spot}/T_{\rm photosphere}$, of about 0.80. Spot latitude runs from 0 at the $+z$ pole to π radians at the $-z$ pole. Spot longitudes are 0 in the $+x$ part of the x–z plane (i.e. including the other star) and increase counter-clockwise as seen from positive z. The spot parameters were refined with DC and parameters for five spots are in Table 4. The fifth spot, at the substellar point, is only needed to fit the reflection bump phases. A larger gravity effect could obviate the need for that spot. The bolometric gravity brightening exponents (g) used in the program were 1.0 for the hot star and 0.3 for the giant.

The real significance is in the other four spots that fit the data fairly well in all bands, as tidal distortion does not greatly affect the spot parameters. Therefore we list spot solutions only for $q = 4.0$. Spots applied to model radial velocity curves had noticeable effects on fitting and could partly account for some of the stray velocity points in our data. Spots were not considered in the overall velocity solutions since the various epochs would have seen changes in spot activity. From the point of view of radiative physics, magnetic spots are likely seats of emission line behaviour that could contribute to the intricate fluorescent emission of the next section.

Table 3. FF Aqr simultaneous solutions of two velocity sets and the 1975-6 *U* light curve, for three mass ratios.

Parameter	Value	Value	Value
q	3.5	4.0	4.5
T_0 (HJD_0)	244 2752.95500±0.00044	244 2752.95440±0.00035	244 2752.95440±0.00032
P (d)	$9\overset{\rm d}{.}208030 \pm 0.000039$	$9\overset{\rm d}{.}208030 \pm 0.000035$	$9\overset{\rm d}{.}208030 \pm 0.000034$
$a/R_\odot$	20.07±0.44	22.16±0.44	24.17±0.47
V_γ (km s^{-1})	25.67±0.39	25.67±0.35	25.67±0.34
i	$73\overset{\circ}{.}68 \pm 0.01$	$75\overset{\circ}{.}97 \pm 0.01$	$77\overset{\circ}{.}97 \pm 0.01$
Ω_1	132.38±1.16	143.60±1.13	154.90±1.17
r_1	0.00776±0.00007	0.00716±0.00006	0.00665±0.00005
Ω_2	10.110	12.500	15.160
r_2 (pole)	0.33614	0.30666	0.28217
r_2 (point)	0.35411	0.31745	0.28916
r_2 (side)	0.34493	0.31247	0.28620
r_2 (back)	0.35024	0.31557	0.28814
Physical radii and masses			
$R_1/R_\odot$	0.156 ± 0.004	0.159 ± 0.003	0.161 ± 0.003
$R_2/R_\odot$	6.90	6.90	6.90
$M_1/M_\odot$	0.29 ± 0.02	0.35 ± 0.02	0.41 ± 0.03
$M_2/M_\odot$	1.00 ± 0.07	1.34 ± 0.09	1.84 ± 0.11

Table 4. FF Aqr spot solutions in 1998 data for $q = 4.0$.

Spot No	Co-latitude (radians)	Longitude (radians)	Ang. radius (radians)	Temp. factor $\frac{T_{\rm spot}}{T_{\rm photosphere}}$
1	0.16±0.06	2.28±0.28	0.39±0.08	0.73±0.04
2	0.61±0.06	4.52±0.02	0.63±0.02	0.81±0.02
3	1.92±0.24	4.50±0.01	0.35±0.09	0.83±0.04
4	1.92±0.04	1.01±0.01	0.58±0.02	0.82±0.01
5	1.57±0.07	6.00±0.07	0.38±0.02	0.81±0.02

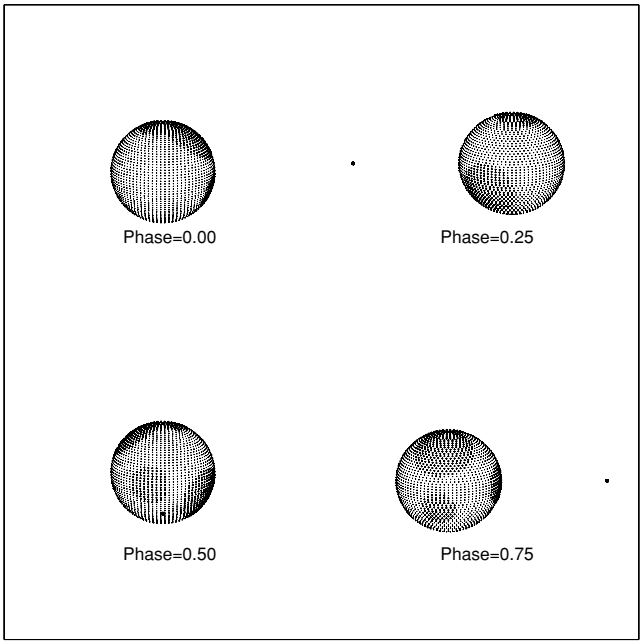

Figure 4. Scaled pictures of FF Aqr that show the spots used in our models. Images were made with the light-curve program.

Graphic models covering key orbital phases show the spot coverage and system scale in Fig. 4, with the four-band light-curve solutions in the panels of Fig. 5. Our differential photometry is in Tables 5–8, where ΔB, ΔV, etc., refer to magnitude differences between FF Aqr and BD -3°5358.

4 BLENDED FLUORESCENT AND PHOTOSPHERIC LINE PROFILES – MODEL VERSUS OBSERVATIONS

The irradiated fluorescent region of the giant has angular radius 76°, as measured at the centre of the star. Our procedure for a first reconnaissance of chromospheric radiation was to generate blended Hα absorption/emission profiles at the observed phases and to use them as templates to evaluate contributions of photospheric absorption and chromospheric emission. The absorption profile at $\phi = 0.95$ p was fit by inspection to establish the absorption profile for the non-irradiated photosphere, with an estimated equivalent width of 0.15 Å. Maximum emission is seen at $\phi = 0.52$ and the equivalent width of the Hα emission line was set at 1.15 Å in our attempt to fit the overall absorption/emission feature. Profiles for other phases were then computed with these set parameters for the absorbing

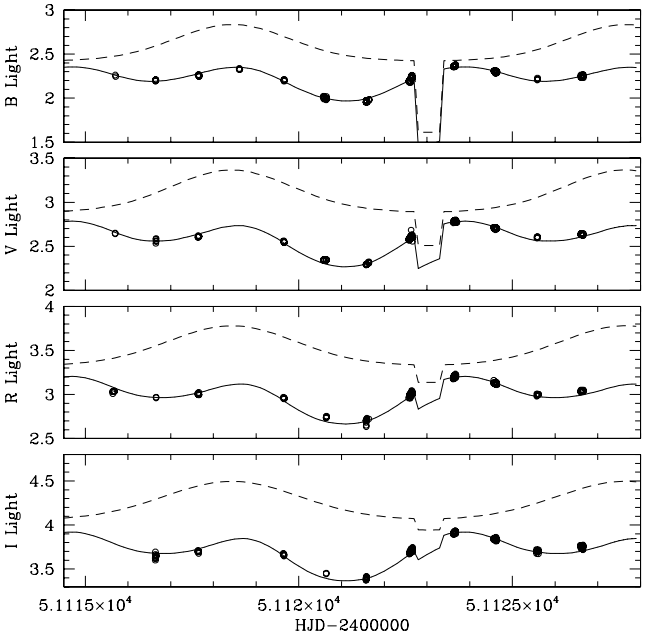

Figure 5. Light-curve model (solid lines) compared with our photometry (open circles). Dashed curves are for an unspotted model and show the reflection bump without contamination by spot effects.

and emitting zones. We stress that these experiments were only exploratory.

There were no significant variations in our spectra during a given night, so only the best spectrum from each night is compared with a profile model in Figs 6, 7 and 8. Our model of fluorescent emission superposed on photospheric absorption provides a template to indicate the width and position of a hypothetical rotationally broadened feature that follows local radial velocity. A template was made also for the morphologically similar binary V471 Tauri, and a preliminary report of that work is in Vaccaro & Wilson (2002). There is partial correspondence between model and spectra that can best be appreciated by viewing a motion picture of observed and theoretical spectral development over V471 Tau's orbital cycle. (Unfortunately it is not practical to show the motion picture in the journal; however, an animation can be found online at http://www.astro.ufl.edu/~vaccaro/V471movie.gif.) For FF Aqr, a broad emission complex was noted by Marilli et al. (1995) whose Hα spectra consistently showed it in the 1990 season but only occasionally in 1991. Our impression from the new spectra is of several blended features that are partly separated at some phases and thoroughly superposed at others. At best we might say that our computed profiles roughly correspond in width with partially resolved components at some phases. We consider the overall mechanism to be related to red giant activity because of the transient behaviour of the profile. There may be a connection with spots because major spot areas are centred on the facing hemisphere near each quadrature according to the light-curve solutions. Spot regions are on the approaching and receding limbs during inferior conjunction of the hot star. Large extended and stable coronal loops anchored to these spots could be forced to corotate with the star and give rise to the additional Doppler broadening. Because such coronal loops seem necessary to account for the large Doppler excursions, we did not place emission regions on the model spots [item (ii) of Section 3.2]. Coronal loops are not included in our line

Table 5. Photometric *B* Data for FF Aqr.

HJD −245 1100	Δ*B*	HJD −245 1100	Δ*B*	HJD −245 1100	Δ*B*	HJD −245 1100	Δ*B*	HJD −245 1100	Δ*B*
15.70823	−0.886	20.59062	−0.760	22.60269	−0.856	23.63455	−0.929	24.61818	−0.899
15.71219	−0.878	20.59581	−0.753	22.60366	−0.848	23.63540	−0.932	24.61904	−0.908
16.64687	−0.859	20.59656	−0.757	22.60987	−0.848	23.63627	−0.931	24.62346	−0.899
16.64784	−0.860	20.59728	−0.755	22.61083	−0.850	23.64148	−0.936	24.62431	−0.898
16.64873	−0.860	20.64236	−0.746	22.61181	−0.844	23.64233	−0.934	24.62517	−0.903
16.64961	−0.853	20.64309	−0.753	22.62182	−0.870	23.64319	−0.936	24.62966	−0.905
16.65059	−0.860	20.64383	−0.742	22.62279	−0.871	23.64854	−0.936	24.63050	−0.902
16.65149	−0.854	20.64915	−0.750	22.62375	−0.867	23.64941	−0.935	24.63136	−0.902
16.65244	−0.861	20.64990	−0.752	22.63139	−0.870	23.65026	−0.934	24.63578	−0.905
16.65336	−0.857	20.65062	−0.762	22.63236	−0.870	23.65967	−0.935	24.63664	−0.905
17.64544	−0.886	21.57867	−0.729	22.63333	−0.869	23.65967	−0.935	24.63748	−0.899
17.64687	−0.886	21.57975	−0.726	22.63759	−0.871	23.66052	−0.936	25.58725	−0.863
17.66414	−0.878	21.58072	−0.729	22.63856	−0.875	23.66137	−0.936	25.58787	−0.859
17.66558	−0.881	21.58643	−0.737	22.63952	−0.871	23.66633	−0.942	25.59181	−0.870
17.66701	−0.883	21.58753	−0.738	22.64245	−0.876	23.66719	−0.935	25.59244	−0.864
17.66845	−0.888	21.58850	−0.740	22.64342	−0.873	23.66804	−0.942	25.59305	−0.864
17.66988	−0.879	21.59754	−0.726	22.64438	−0.880	23.67291	−0.942	26.60388	−0.886
18.60507	−0.917	21.59851	−0.729	22.64716	−0.883	23.67377	−0.937	26.60451	−0.873
18.60651	−0.922	21.59947	−0.734	22.64813	−0.885	23.67461	−0.932	26.60512	−0.880
18.61357	−0.916	21.64749	−0.739	22.64911	−0.883	24.56977	−0.908	26.61619	−0.877
18.61500	−0.917	21.64845	−0.745	22.65239	−0.877	24.57517	−0.908	26.61682	−0.878
19.65029	−0.858	21.64942	−0.744	22.65337	−0.878	24.57602	−0.909	26.61743	−0.872
19.65149	−0.860	22.57867	−0.852	22.65433	−0.870	24.57688	−0.906	26.65066	−0.887
19.65270	−0.856	22.57965	−0.848	22.65942	−0.871	24.59676	−0.897	26.65128	−0.878
19.66079	−0.852	22.58062	−0.855	22.66039	−0.874	24.59726	−0.905	26.65190	−0.886
19.66199	−0.862	22.58652	−0.850	22.66135	−0.871	24.59776	−0.907	26.65634	−0.882
19.66319	−0.858	22.58774	−0.851	23.62028	−0.930	24.60296	−0.900	26.65695	−0.871
20.58189	−0.761	22.58871	−0.855	23.62138	−0.931	24.60382	−0.899	26.65758	−0.888
20.58289	−0.759	22.59454	−0.853	23.62223	−0.932	24.60467	−0.902	26.66193	−0.879
20.58362	−0.765	22.59551	−0.857	23.62767	−0.934	24.61028	−0.896	26.66254	−0.880
20.58915	−0.748	22.59647	−0.854	23.62853	−0.932	24.61289	−0.911	26.66317	−0.882
20.58989	−0.756	22.60172	−0.854	23.62938	−0.932	24.61732	−0.906		

profile model and radial velocities of regions immediately above spots would be unlikely to differ much from the underlying photospheric velocities.

Similar emitting sources have been investigated for the fast rotating K dwarf AB Doradus by Cameron & Robinson (1989a,b), who observed transient Balmer emission and absorption moving through the stellar absorption profile. Emission was seen on the blue and red wings and additional absorption travelled across the profile. The features were identified as extended structures that emitted when away from the limb and absorbed when projected over the facing hemisphere. Their model was of neutral gas trapped by ionized gas in magnetic loops extending several stellar radii above the surface and forced to corotate. These clouds persisted for a good portion of the 12.5-h cycle. Clouds that existed for more than four rotations are noted by Donati et al. (1999), who modelled AB Dor's circumstellar magnetic field, as did Jardine et al. (1999). UV spectroscopy of AB Dor (Vilhu et al. 1998) has turned up a wealth of strong emissions that can help diagnose the overall situation. If the AB Dor model applies also to FF Aqr, we might expect additional sources of fluorescence facing or nearly facing the hot star. If the structures are associated with polar spots then they may partially fill the absorption seen around the eclipse, as they could be visible over the entire orbit. A problem with this interpretation is that we do not see a transition from blueshifted to redshifted profiles that would indicate rotation. Perhaps this is due to the lifetimes of these structures being much shorter than the orbital period. More phase redundancy in the observations would be needed to examine this issue further.

Additional support for extended regions above the red giant surface comes from Baliunas et al. (1986), who observed absorption lines of species such as C II and C IV that doubled in strength during ingress and egress of the hot star eclipse, relative to quadrature. They suggest that the excess absorption is caused by a geometrically extended region of the giant and that the enhancements are present to at least 1.5 stellar radii above its surface. However, they believe the phenomena to be permanent as the enhancements persisted for three years. The multiple emission components are more difficult to understand. At phase $\phi = 0.85$ the impression is of one broad feature, but more often we see a blended pair.

Mass transfer or loss can affect a binary orbit. Etzel et al. (1988) states that P has undergone a sudden increase, based on a revised spectroscopic orbit and photometry from 1986 and 1987, but without published numbers. The stars in FF Aqr are well within their limiting lobes so there should be no mass transfer by lobe overflow. A P increase due to conservative mass transfer is implausible, as it would require the low-mass star to transfer mass to the giant. Mass loss from the system could cause a P increase. Although no significant $\mathrm{d}P/\mathrm{d}t$ was found in our analysis, a change in P from that given by Dworetsky et al. (1977) is apparent. If the P change is real,

Table 6. Photometric V data for FF Aqr.

HJD −245 1100	ΔV	HJD −245 1100	ΔV	HJD −245 1100	ΔV	HJD −245 1100	ΔV	HJD −245 1100	ΔV
15.70287	−1.058	20.64168	−0.921	22.62013	−1.045	23.65802	−1.106	24.62281	−1.083
15.70730	−1.055	20.64733	−0.926	22.62058	−1.040	23.65846	−1.116	24.62812	−1.081
16.65490	−1.029	20.64784	−0.926	22.62102	−1.034	23.66474	−1.112	24.62856	−1.080
16.65570	−1.009	20.64833	−0.927	22.62974	−1.039	23.66518	−1.107	24.62901	−1.079
16.65626	−1.022	21.57690	−0.902	22.63018	−1.039	23.66563	−1.114	24.63425	−1.081
16.65901	−1.033	21.57740	−0.900	22.63062	−1.072	23.67130	−1.107	24.63469	−1.077
16.65970	−1.018	21.57791	−0.901	22.63590	−1.041	23.67175	−1.118	24.63513	−1.080
17.64164	−1.039	21.58461	−0.901	22.63635	−1.048	23.67219	−1.115	25.58060	−1.035
17.64282	−1.046	21.58512	−0.904	22.63679	−1.049	23.69779	−1.109	25.58098	−1.040
17.64392	−1.039	21.58562	−0.899	22.64153	−1.044	23.69824	−1.106	25.59054	−1.042
17.65913	−1.044	21.59312	−0.904	22.64631	−1.048	23.69868	−1.109	25.59092	−1.038
17.65999	−1.043	21.59363	−0.902	22.65159	−1.045	24.56739	−1.084	25.59130	−1.037
17.66084	−1.041	21.59412	−0.903	22.65864	−1.048	24.56783	−1.084	26.60247	−1.055
17.66169	−1.040	21.63959	−0.912	22.66559	−1.019	24.56827	−1.085	26.60285	−1.050
17.66254	−1.044	21.64010	−0.916	22.66604	−1.038	24.57364	−1.083	26.60324	−1.052
19.64748	−1.019	21.64060	−0.908	22.66648	−1.038	24.57409	−1.079	26.60984	−1.052
19.64821	−1.019	22.57672	−1.027	23.61845	−1.105	24.57453	−1.084	26.61023	−1.053
19.64895	−1.022	22.57722	−1.027	23.61906	−1.109	24.59536	−1.085	26.61062	−1.057
19.65823	−1.015	22.57771	−1.028	23.61951	−1.108	24.59581	−1.082	26.64902	−1.051
19.65896	−1.013	22.58451	−1.032	23.62607	−1.114	24.59626	−1.084	26.64941	−1.056
19.65970	−1.014	22.58500	−1.025	23.62651	−1.112	24.60138	−1.084	26.64979	−1.048
20.57918	−0.924	22.58551	−1.030	23.62697	−1.107	24.60182	−1.074	26.65506	−1.050
20.58023	−0.926	22.59285	−1.031	23.63250	−1.115	24.60227	−1.078	26.65544	−1.049
20.58096	−0.923	22.59329	−1.028	23.63294	−1.112	24.60760	−1.084	26.65582	−1.046
20.58711	−0.925	22.59373	−1.033	23.63339	−1.111	24.60805	−1.082	26.66065	−1.056
20.58762	−0.928	22.59983	−1.028	23.63973	−1.113	24.60898	−1.081	26.66103	−1.050
20.59411	−0.922	22.60027	−1.031	23.64018	−1.111	24.61578	−1.079	26.66141	−1.052
20.59462	−0.922	22.60072	−1.029	23.64063	−1.111	24.61624	−1.078		
20.59512	−0.922	22.60818	−1.040	23.64692	−1.112	24.61667	−1.083		
20.64067	−0.927	22.60862	−1.034	23.64736	−1.115	24.62193	−1.078		
20.64117	−0.925	22.60906	−1.029	23.64781	−1.114	24.62237	−1.078		

possible mass loss suggested by our spectra may be a key contributor. An upper estimate of this mass loss ($\dot{M}_2$) can be made with

$$\frac{\dot{P}}{P} = -\frac{2\dot{M}_2}{M_1 + M_2}, \tag{2}$$

if we assume an isotropic wind from the giant star (Pringle 1985). We can postulate a rough maximum $\dot{P}$ based on the 1σ uncertainty in our $q = 4.0$ solution, whereby $\dot{P} \approx 10^{-7}$. With our $M_{1,2}$ of Table 3, we find $\dot{M}_2 \approx 3 \times 10^{-6}$ $M_\odot$ yr^{-1}. This mass-loss rate falls in the range of measured values for hot and cool luminous supergiants (Bohm-Vitense 1989). This seems implausibly – although perhaps not impossibly – high for FF Aqr's giant, but may be enhanced by binary effects, as suggested by Tout & Eggleton (1988), although their ideas most directly concern an earlier evolutionary stage than that of the present FF Aqr. A dense wind could lend support to the extended atmosphere observed by Baliunas et al. (1986). Possibly a combination of these and other mechanisms could produce the spectral complexities. More thorough analysis must await spectral coverage that extends over at least several orbits.

5 NATURE OF THE HOT STAR

Most FF Aqr contributions refer to the hot star as a subdwarf, thereby adopting the relatively recent empirical definition of a hot subdwarf as any hot star between the Population I main sequence and the white dwarfs. Some of the stars in that region are on the helium main sequence, some are helium stars with thin outer envelopes of normal composition, and some are contracting toward the helium main sequence or toward a white dwarf state. More traditionally, subdwarfs are hydrogen-burning main-sequence stars of low metallicity and, while hot subdwarfs can exist under the traditional definition, they have to be massive, whereas a traditional subdwarf of $M \approx 0.4$ $M_\odot$ (Table 2) would be cooler than the Sun. We prefer to maintain distinctions among such stars in naming as well as in evolutionary terms so we avoid the name 'subdwarf' for the primary of FF Aqr. The star cannot be a white dwarf because it is too large at $R \approx 0.16$ $R_\odot$. The radius is not very accurately pinned down but if it were of white dwarf size, the light curve of Dworetsky et al. (1977) almost certainly would not have captured so many data points (about 25 to 30) in the brief partial phases. We cannot check this point directly, as our scan of the plot of Dworetsky et al. lacks sufficient phase resolution, but Dworetsky et al. estimated the hot star radius to be 0.11 $R_\odot$ from eclipse contact timings, which is far beyond white dwarf size. Helium star models of 0.4 $M_\odot$ (Kippenhahn & Weigert 1990) are smaller ($R \approx 0.08$ $R_\odot$) and cooler ($T_{\rm eff} \approx 30\,000$ K) than the estimates of Table 3, but possibly not outside the range of observational uncertainty. The star may be contracting *toward* a helium star or white dwarf state, in which case the brevity of any contraction stage would place strong constraints on the prior binary evolution. We would then have to say that the original masses were quite similar so that the evolution of the present giant star has not lagged very far behind that of the primary; see also the comment by Dworetsky et al. (1977) on time-scales.

Table 7. Photometric *R* data for FF Aqr.

HJD −245 1100	Δ*R*	HJD −245 1100	Δ*R*	HJD −245 1100	Δ*R*	HJD −245 1100	Δ*R*	HJD −245 1100	Δ*R*
15.64487	−1.206	21.57582	−1.079	22.65094	−1.206	23.66982	−1.274	24.62731	−1.241
15.64548	−1.204	21.57626	−1.079	22.65799	−1.204	23.67021	−1.271	24.62769	−1.236
15.64655	−1.196	21.58300	−1.072	22.66428	−1.194	23.67060	−1.269	24.63305	−1.237
15.68287	−1.206	21.58362	−1.058	22.66466	−1.193	23.67646	−1.264	24.63343	−1.234
15.68332	−1.205	21.58407	−1.052	22.66504	−1.197	23.67685	−1.262	24.63383	−1.232
15.68378	−1.207	21.59168	−1.085	23.61572	−1.255	23.67723	−1.270	25.57513	−1.195
16.66061	−1.182	21.59212	−1.087	23.61674	−1.256	24.56618	−1.238	25.57547	−1.186
16.66115	−1.179	21.59257	−1.090	23.61715	−1.256	24.56656	−1.249	25.58945	−1.190
17.63866	−1.194	21.63904	−1.087	23.61757	−1.261	24.56696	−1.238	25.58981	−1.189
17.63927	−1.195	22.57525	−1.179	23.62454	−1.264	24.57242	−1.240	25.59016	−1.195
17.63990	−1.198	22.59140	−1.190	23.62517	−1.262	24.57281	−1.239	25.61077	−1.194
17.64051	−1.194	22.59179	−1.190	23.62557	−1.262	24.57320	−1.240	25.61113	−1.194
17.65552	−1.195	22.59217	−1.192	23.63122	−1.261	24.59413	−1.237	25.61148	−1.191
17.65613	−1.201	22.59858	−1.185	23.63162	−1.260	24.59452	−1.237	26.60140	−1.204
17.65675	−1.192	22.59896	−1.191	23.63201	−1.265	24.59492	−1.242	26.60175	−1.203
17.65737	−1.193	22.59934	−1.187	23.63838	−1.269	24.59908	−1.237	26.60210	−1.209
17.65800	−1.191	22.60729	−1.180	23.63877	−1.265	24.59947	−1.241	26.60867	−1.210
19.64264	−1.176	22.60773	−1.177	23.63916	−1.266	24.59985	−1.236	26.60903	−1.211
19.64314	−1.182	22.61888	−1.197	23.64563	−1.264	24.60678	−1.240	26.60938	−1.206
19.65646	−1.176	22.61926	−1.196	23.64601	−1.267	24.60717	−1.233	26.64830	−1.205
19.65696	−1.178	22.61965	−1.197	23.64641	−1.268	24.61458	−1.239	26.64864	−1.209
19.65746	−1.175	22.62848	−1.196	23.65670	−1.263	24.61496	−1.243	26.65398	−1.204
20.63918	−1.093	22.62887	−1.197	23.65709	−1.267	24.61536	−1.237	26.65433	−1.210
20.64589	−1.092	22.62926	−1.199	23.65747	−1.266	24.62073	−1.234	26.65469	−1.206
20.64633	−1.098	22.63531	−1.195	23.66327	−1.269	24.62111	−1.239	26.65957	−1.211
20.64677	−1.100	22.64104	−1.203	23.66365	−1.269	24.62150	−1.241	26.65992	−1.210
21.57536	−1.082	22.64585	−1.209	23.66403	−1.258	24.62685	−1.238	26.66026	−1.204

Table 8. Photometric *I* data for FF Aqr.

HJD −245 1100	Δ*I*	HJD −245 1100	Δ*I*	HJD −245 1100	Δ*I*	HJD −245 1100	Δ*I*	HJD −245 1100	Δ*I*
16.64214	−1.391	21.58163	−1.321	22.66383	−1.434	24.57133	−1.462	25.56919	−1.421
16.64409	−1.419	21.58201	−1.326	23.62390	−1.477	24.57168	−1.459	25.57083	−1.414
16.64458	−1.396	21.58239	−1.324	23.63007	−1.483	24.57204	−1.464	25.57114	−1.427
16.64503	−1.410	21.58959	−1.334	23.63043	−1.475	24.59295	−1.460	25.58848	−1.419
16.64558	−1.399	21.58997	−1.331	23.63078	−1.482	24.59339	−1.460	25.58879	−1.421
16.64600	−1.401	21.59036	−1.326	23.63699	−1.479	24.59375	−1.461	25.58911	−1.425
16.66207	−1.407	22.59039	−1.412	23.63735	−1.482	24.60059	−1.461	25.60920	−1.413
16.66251	−1.405	22.59073	−1.415	23.63771	−1.478	24.60094	−1.460	25.61011	−1.426
17.63671	−1.419	22.59735	−1.416	23.64387	−1.478	24.60530	−1.461	25.61043	−1.420
17.63721	−1.420	22.59771	−1.421	23.64422	−1.485	24.60566	−1.464	26.59705	−1.441
17.63771	−1.424	22.59806	−1.417	23.64458	−1.479	24.60600	−1.464	26.59954	−1.440
17.65260	−1.419	22.61773	−1.418	23.65473	−1.482	24.61350	−1.461	26.60038	−1.433
17.65311	−1.414	22.61808	−1.416	23.65509	−1.482	24.61386	−1.463	26.60769	−1.430
17.65361	−1.422	22.61843	−1.416	23.65544	−1.486	24.61421	−1.456	26.60800	−1.440
17.65412	−1.419	22.62709	−1.423	23.66205	−1.485	24.61965	−1.467	26.60832	−1.438
17.65462	−1.420	22.62744	−1.428	23.66241	−1.483	24.62000	−1.462	26.64668	−1.440
19.63998	−1.409	22.62780	−1.422	23.66277	−1.487	24.62034	−1.454	26.64705	−1.438
19.64086	−1.414	22.63414	−1.427	23.66870	−1.480	24.62578	−1.460	26.64736	−1.428
19.65377	−1.405	22.63449	−1.429	23.66906	−1.479	24.62613	−1.461	26.65301	−1.432
19.65490	−1.409	22.63485	−1.426	23.66940	−1.487	24.62649	−1.456	26.65332	−1.442
19.65529	−1.411	22.64062	−1.423	23.67534	−1.478	24.63197	−1.458	26.65363	−1.426
20.64487	−1.346	22.64536	−1.430	23.67569	−1.485	24.63233	−1.459	26.65889	−1.438
20.64525	−1.343	22.65048	−1.428	23.67604	−1.482	24.63268	−1.460	26.65921	−1.438
21.57271	−1.329	22.65757	−1.430	24.56509	−1.462	25.56699	−1.420		
21.57374	−1.320	22.66312	−1.419	24.56545	−1.459	25.56763	−1.422		
21.57465	−1.324	22.66347	−1.420	24.56580	−1.463	25.56797	−1.422		

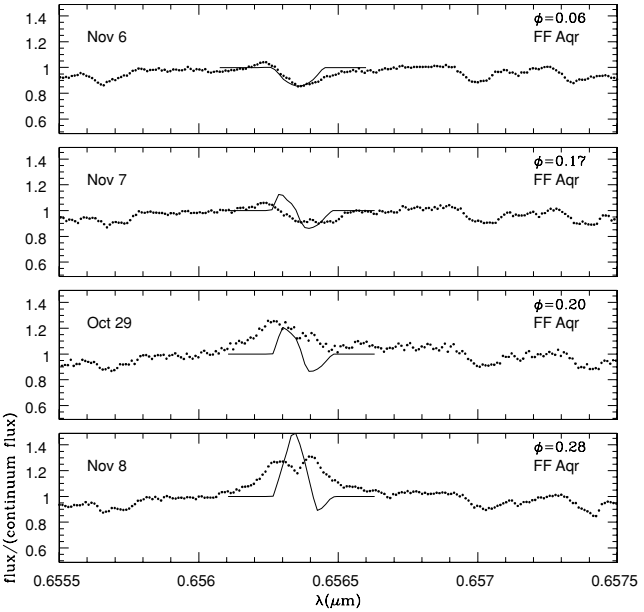

Figure 6. Observed spectra of FF Aqr (dotted line) and the modelled Hα profile (solid line) for phases 0.06–0.28.

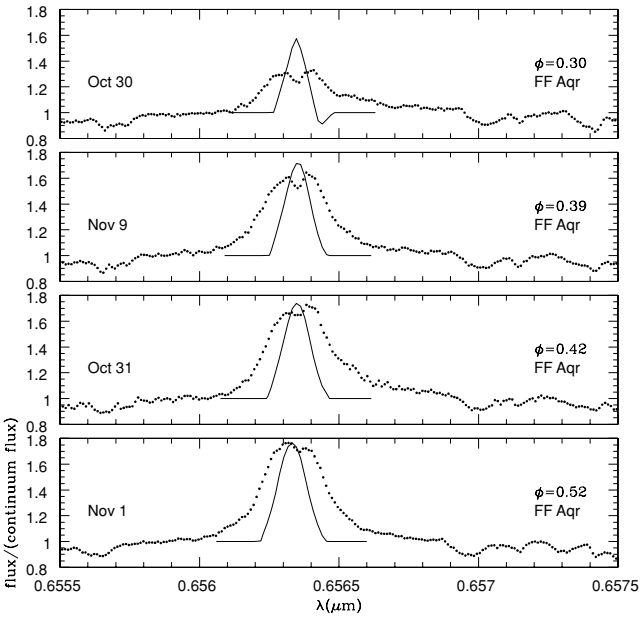

Figure 7. Observed spectra of FF Aqr (dotted line) and the modelled Hα profile (solid line) for phases 0.30–0.52.

6 CONCLUSIONS

The numerous spots and additional Hα emission in addition to the expected fluorescence indicate that FF Aqr was highly active in 1998. Spots modelled on the sides of the star may anchor large corotating coronal loops that also fluoresce, thereby broadening the observed Hα profile. These structures would normally be associated with magnetic braking but could also provide means of mass loss or transfer and affect P. A large spot region on the facing hemisphere seen near phase 0.8 may be the site of emission associated with mass ejection and cause ongoing period changes.

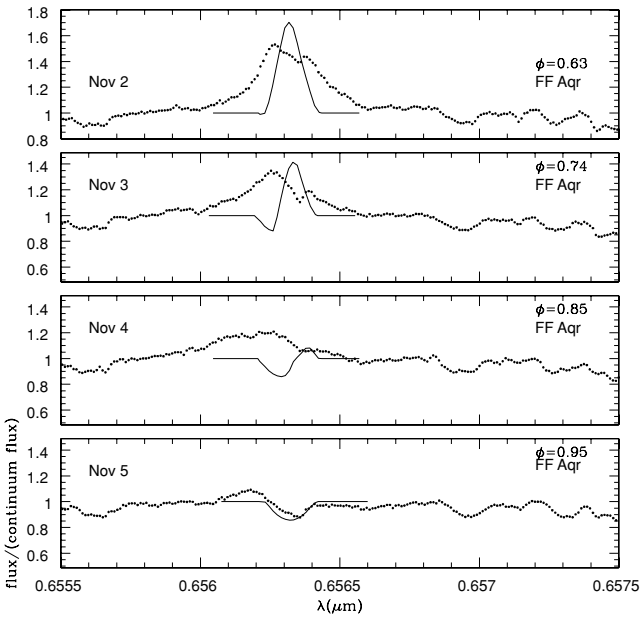

Figure 8. Observed spectra of FF Aqr (dotted line) and the modelled Hα profile (solid line) for phases 0.63–0.95.

ACKNOWLEDGMENTS

We thank KPNO and SARA for granting observing time. We are especially grateful for the observing support of Walter Van Hamme, Rolando Branley, Peter Mack and Gerrie Peters. We also thank A. Frasca for providing some of the radial velocities, and the referees for helpful suggestions. This work was supported in part by NSF grant AST-097895 (A. U. Landolt Principal Investigator) to Louisiana State University.

REFERENCES

Allen C. W., 2000, in Cox A. N., ed., Astrophysical Quantities, 4th edn. AIP Press, New York, p. 388
Baliunas S. L., Loesser J. G., Raymond J. C., Guinan E. F., Dorren J. D., 1986, in Proc. ESA Int. Symp. on New Insights in Astrophysics, Eight Years of UV Astronomy with, *IUE*. ESA Publications Division, Noordwijck, p. 185
Bohm-Vitense E., 1989, Introduction to Stellar Astrophysics, Vol. 2. Cambridge Univ. Press, Cambridge, p. 215
Bopp B. W., Talcott J. C., 1980, AJ, 85, 55
Cameron A. C., Robinson R., 1989a, MNRAS, 236, 57
Cameron A. C., Robinson R., 1989b, MNRAS, 238, 657
Carnochan D. J., Dworetsky M. M., Todd J. J., Willis A. J., Wilson R., 1975, R. Soc. Philos. Trans. Ser. A, 279, 479
Donati J. F., Cameron A. C., Hussain G. A. J., Semel M., 1999, MNRAS, 302, 437
Dorren J. D., Guinan E. F., Siah M. J., 1983, IBVS, 2305
Dworetsky M. M., Lanning H. H., Etzel P. E., Patenaude D. J., 1977, MNRAS, 181, 13
Etzel P., 1989, BAAS Ann. Rep., 21, 567
Etzel P. B., Lanning H. H., Dworetsky M. M., Hamilton I., 1988, BAAS, 20, 912
Jardine M., Barnes J. R., Donati J., Cameron C., 1999, MNRAS, 305, L35
Kippenhahn R., Weigert A., 1990, Stellar Structure and Evolution. Springer-Verlag Berlin, ch. 23
Marilli E., Frasca A., Bellina-Terra M., Catalano S., 1995, A&A, 295, 393
Marilli E., Frasca A., Catalano S., Bellina-Terra M., 1996, in Pallavicini R., Dupree A. K. eds, ASP Conf. Ser. Vol. 109, Cool Stars, Stellar Systems, and the Sun. Astron. Soc. Pac., San Francisco, p. 653

Pringle J. E., 1985, in Pringle J. E., Wade R. A., eds, Interacting Binary Stars. Cambridge Univ. Press, Cambridge, p. 1
Tout C. A., Eggleton P. P., 1988, MNRAS, 231, 823
Vaccaro T. R., Wilson R. E., 1999a, in Wilson R. E., Hegedus T., Borkovits T., Gimenez A., eds, Proc. Kecskemet Conf. Var. Stars. Alvaro Gimenez Canete, Madrid, p. 113
Vaccaro T. R., Wilson R. E., 1999b, BAAS, 31, 1485
Vaccaro T. R., Wilson R. E., 2002, in Tout C. A., Van Hamme W., eds, ASP Conf. Ser. Vol. 279, Exotic Starsa as Challenges to Evolution. Astron. Soc. Pac., San Francisco, p. 167
Van Hamme W., 1993, AJ, 106, 2096
Vilhu O., Muhli P., Huovelin J., Hakala P., Rucinski S. M., Cameron A. C., 1998, AJ, 115, 1610
Wilson R. E., 1979, ApJ, 234, 1054
Wilson R. E., 1990, ApJ, 356, 613
Wilson R. E., Devinney E. J., 1971, ApJ, 166, 605
Wilson R. E., Sofia S., 1976, ApJ, 203, 182
Young A., Skumanich A., Paylor V., 1988, ApJ, 334, 397

This paper has been typeset from a TEX/LATEX file prepared by the author.